

# Tunable high-resolution synthetic aperture radar imaging

Tsogka Chrysoula<sup>1</sup> and Kim Arnold D<sup>2</sup>

<sup>1</sup>University of California Merced

<sup>2</sup>University of California, Merced

November 16, 2022

## Abstract

We have recently introduced a modification of the multiple signal classification (MUSIC) method for synthetic aperture radar. This method depends on a tunable, user-defined parameter,  $\epsilon$ , that allows for quantitative high-resolution imaging. It requires however, relative large single-to-noise ratios (SNR) to work effectively. Here, we first identify the fundamental mechanism in that method that produces high-resolution images. Then we introduce a modification to Kirchhoff Migration (KM) that uses the same mechanism to produces tunable, high-resolution images. This modified KM method can be applied to low SNR measurements. We show simulation results that demonstrate the features of this method.



**Abstract**

We have recently introduced a modification of the multiple signal classification (MUSIC) method for synthetic aperture radar. This method depends on a tunable, user-defined parameter,  $\epsilon$ , that allows for quantitative high-resolution imaging. It requires however, relative large single-to-noise ratios (SNR) to work effectively. Here, we first identify the fundamental mechanism in that method that produces high-resolution images. Then we introduce a modification to Kirchhoff Migration (KM) that uses the same mechanism to produce tunable, high-resolution images. This modified KM method can be applied to low SNR measurements. We show simulation results that demonstrate the features of this method.

**1 Introduction**

In synthetic aperture radar (SAR) a single transmitter/receiver on a platform is used to probe an imaging region of interest by emitting pulses and then record the subsequent echoes as the platform moves along a flight path. SAR imaging methods use these measurements to reconstruct images of targets in the imaging region of interest.

The traditional SAR image is formed by evaluating the data at each measurement location at the travel time that it takes for the waves to propagate from the platform location to a point in the imaging region on the ground and back. This imaging method is called Kirchhoff Migration (KM). The resolution of the image produced by KM has a range resolution that is  $O(c/B)$  with  $c$  denoting the wave speed, and  $B$  denoting the system bandwidth, and a cross-range resolution that is  $O(\lambda_0 L/a)$  with  $\lambda_0$  denoting the central wavelength,  $L$  denoting the characteristic distance from the platform to the imaging region, and  $a$  denoting the length of the synthetic aperture (Cheney & Borden, 2009).

The authors have recently developed a modification to the multiple signal classification method (MUSIC) for SAR imaging (Kim & Tsogka, 2021). This method includes a user-defined parameter, which we call  $\epsilon$ , that allows for tunable, high-resolution images. Using this method, we obtain a range resolution that is  $O(\sqrt{\epsilon}(c/B)(L/R))$  with  $R$  denoting the range distance from the flight path to the center of the imaging region, and a cross-range resolution of  $O(\sqrt{\epsilon}(c/B)(L/a))$ . The key here is that the user-defined parameter  $\epsilon$  can be made arbitrarily small which, in turn, allows for tunable high-resolution quantitative images. However, this method is limited to measurements with relatively high signal-to-noise ratios (SNRs). Otherwise, one cannot reliably separate signal from noise, which is a key step in this method. The quantitative recovery of reflectivity information suffers most when the SNR becomes too low, but image resolution also suffers.

In many practical applications, SAR data are very noisy (Doerry, 2006). For these problems, the modification to MUSIC will not be effective because the SNR is not sufficiently high. For this reason, we seek to develop a new method that retains the tunable high-resolution feature of this method, but can accommodate measurements with low SNR. To do this, we first re-evaluate the modification to MUSIC and identify the fundamental mechanism leading to tunable high-resolution. This mechanism involves a simple rational transformation. We form the same rational transformation of the normalized KM image and obtain a tunable high-resolution version of the KM method. This method requires no additional computations beyond those required for KM. The result of this modification is a method with a range resolution that is  $O(\sqrt{\epsilon}c/B)$  and a cross-range resolution that is  $O(\sqrt{\epsilon}\lambda_0 L/a)$ .

The remainder of this paper is as follows. In Section 2 we give a brief description of synthetic aperture radar imaging, our assumptions, and define the measurements. In Section 3 we briefly review the recent modification to MUSIC and identify the fundamental mechanism allowing for tunable high-resolution imaging. Using the insight gained

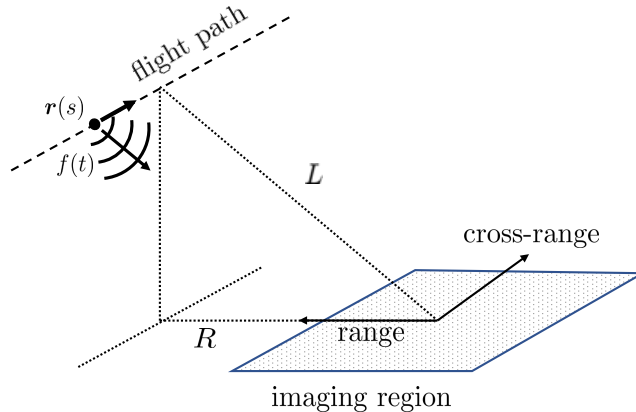


**Figure 1.** Setup for synthetic aperture radar imaging.

60 from identifying this fundamental mechanism, we introduce a modification to KM in Sec-  
 61 tion 4. We show several simulation results in Section 5 that demonstrate the features  
 62 of the modified KM method. Section 6 contains our conclusions.

63 **2 Synthetic aperture radar imaging**

64 We consider synthetic aperture radar (SAR) imaging in which a single transmit-  
 65 ter/receiver on a moving platform emits and records signals (Cheney, 2001; Cheney &  
 66 Borden, 2009; Moreira et al., 2013). A full set of measurements corresponds to a suite  
 67 of experiments at several locations along the flight path. Let  $f(t)$  denote the broadband  
 68 pulse emitted and let  $d(s, t)$  denote the data recorded which depends on the slow time  
 69  $s$  parameterizing the flight path of the platform,  $\mathbf{r}(s)$ , and the fast time  $t$  correspond-  
 70 ing to the round-trip travel time between the platform and the imaging scene. Here, we  
 71 assume the start-stop approximation in which the change in displacement between the  
 72 targets and the platform is negligibly small compared to the travel time it takes for the  
 73 pulse emitted to propagate to the imaging scene and return as echoes.

74 Figure 1 shows an illustration of SAR imaging. Here, we see that range is the co-  
 75 ordinate obtained by projecting the vector that connects the center of the imaging re-  
 76 gion to the central platform location onto the imaging plane, and cross-range is the co-  
 77 ordinate orthogonal to range. Denoting the size of the synthetic aperture by  $a$  and the  
 78 system bandwidth by  $B$ , the typical resolution of the imaging system is  $O((c/B)(L/R))$   
 79 in range and  $O(\lambda L/a)$  in cross-range. Here  $c$  is the speed of light and  $\lambda$  the wavelength  
 80 corresponding to the central frequency while  $L$  denotes the distance between the plat-  
 81 form and the imaging region and  $R$  the offset in range.

82 With the start-stop approximation, measurements are taken at  $N$  discrete values  
 83 of  $s$ , corresponding to  $d(s_n, t)$  for  $n = 1, \dots, N$ . Next, we compute the discrete Fourier  
 84 transform of digitally sampled values of  $d(s_n, t)$  in  $t$  denoted by  $d_n(\omega_m)$  for  $m = 1, \dots, 2M -$   
 85 1. The full set of measurements is the  $2M - 1 \times N$  matrix  $D$  whose columns are

$$\mathbf{d}_n = \begin{bmatrix} d_n(\omega_1) \\ d_n(\omega_2) \\ \vdots \\ d_n(\omega_{2M-1}) \end{bmatrix}, \quad n = 1, \dots, N. \tag{1}$$

86 The objective in SAR imaging is to identify and locate targets in an imaging region us-  
87 ing these data.

### 88 3 MUSIC for SAR

89 The authors have recently extended MUSIC for SAR resulting in a tunable, quan-  
90 titative high-resolution imaging method (Kim & Tsogka, 2021). The main limitation of  
91 this method is that it requires sufficiently high SNR to distinguish between signal and  
92 noise subspaces. We review this method here and identify the key mechanism that leads  
93 to tunable high-resolution images.

94 The key to applying MUSIC to SAR is a reorganization of the data matrix  $D$  which  
95 we explain below. Consider the  $n$ th column of  $D$  given in (1). Applying the Prony method (Prony,  
96 1795) to this vector of length  $2M - 1$  yields the following  $M \times M$  matrix,

$$D_n = \begin{bmatrix} d_n(\omega_1) & d_n(\omega_2) & \cdots & d_n(\omega_M) \\ d_n(\omega_2) & d_n(\omega_3) & \cdots & d_n(\omega_{M+1}) \\ \vdots & \vdots & \ddots & \vdots \\ d_n(\omega_M) & d_n(\omega_{M+1}) & \cdots & d_n(\omega_{2M-1}) \end{bmatrix}. \quad (2)$$

97 In this rearrangement, the first column is the truncation of  $\mathbf{d}_n$  to its first  $M$  entries. Sub-  
98 sequent columns are sequential upward shifts of  $\mathbf{d}_n$  truncated to its first  $M$  entries.

99 When there is no measurement noise and the frequencies are sampled at a fixed  
100 rate, (2) can be factorized as a sum of outer products, each corresponding to an indi-  
101 vidual point target (Kim & Tsogka, 2021). Suppose there are  $K$  point targets in the imag-  
102 ing region located at positions  $\mathbf{y}_k$  with reflectivities  $\rho_k$  for  $k = 1, \dots, K$ . It follows that

$$D_n = \sum_{k=1}^K s_k^{(n)} \mathbf{u}_k^{(n)} \mathbf{v}_k^{(n)H}, \quad (3)$$

with  $s_k^{(n)} = \rho_k / (4\pi |\mathbf{x}_n - \mathbf{y}_k|)^2$ ,

$$\mathbf{u}_k^{(n)} = \begin{bmatrix} e^{i2\omega_1 |\mathbf{x}_n - \mathbf{y}_k|/c} \\ e^{i2\omega_2 |\mathbf{x}_n - \mathbf{y}_k|/c} \\ \vdots \\ e^{i2\omega_M |\mathbf{x}_n - \mathbf{y}_k|/c} \end{bmatrix}, \quad \text{and} \quad \mathbf{v}_k^{(n)} = \begin{bmatrix} 1 \\ e^{-i2\Delta\omega |\mathbf{x}_n - \mathbf{y}_k|/c} \\ \vdots \\ e^{-i2(M-1)\Delta\omega |\mathbf{x}_n - \mathbf{y}_k|/c} \end{bmatrix}. \quad (4)$$

103 Here,  $\mathbf{x}_n$  denotes the platform location at the  $n$ th measurement,  $\omega_m = \omega_1 + (m-1)\Delta\omega$   
104 for  $m = 1, \dots, M$ , and  $c$  denotes the wave speed.

105 Assuming that  $K < M$ , we find that the column space of  $D_n$  is given by

$$\mathcal{S} = \text{span}\{\mathbf{u}_1^{(n)}, \dots, \mathbf{u}_K^{(n)}\}, \quad (5)$$

106 which corresponds to the signal subspace. Upon computing the singular value decom-  
107 position  $D_n = U\Sigma V^H$ , we find that the first  $K$  columns of  $U$  give an orthonormal basis  
108 for  $\mathcal{S}$ . Let  $\tilde{U}$  be the  $M \times K$  matrix corresponding to the first  $K$  columns of  $U$ . The  
109 projection onto the signal subspace is then  $P_{\text{signal}} = \tilde{U}\tilde{U}^H$ . The noise subspace is the  
110 orthogonal complement to the signal subspace. The projection onto the noise subspace  
111 is  $P_{\text{noise}} = I_M - \tilde{U}\tilde{U}^H$  with  $I_M$  denoting the  $M \times M$  identity matrix.

112 Now suppose we wish to test if a search point  $\mathbf{y}$  somewhere in the imaging region  
113 corresponds to a target. We introduce the illumination vector,

$$\mathbf{a}_n(\mathbf{y}) = \begin{bmatrix} e^{i2\omega_1|\mathbf{x}_n-\mathbf{y}|/c} \\ e^{i2\omega_2|\mathbf{x}_n-\mathbf{y}|/c} \\ \vdots \\ e^{i2\omega_M|\mathbf{x}_n-\mathbf{y}|/c} \end{bmatrix}. \quad (6)$$

114 In traditional MUSIC we form an image by testing if this illumination vector lies in the  
 115 noise subspace. For this case, we compute  $\|P_{\text{noise}}\mathbf{a}_n(\mathbf{y})\|^2$  for  $n = 1, \dots, N$ , and form  
 116 an image by plotting

$$I(\mathbf{y}) = \left[ \sum_{n=1}^N \|P_{\text{noise}}\mathbf{a}_n(\mathbf{y})\|^2 \right]^{-1}. \quad (7)$$

117 The basic idea behind this formation of an image is that when  $\mathbf{y}$  corresponds to a tar-  
 118 get location, the projection onto the noise subspace will be zero, so plotting the recip-  
 119 rocal will yield a singularity there.

120 In the recent modifications to MUSIC (González-Rodríguez et al., 2021; Kim & Tsogka,  
 121 2021), both  $P_{\text{noise}}$  and  $P_{\text{signal}}$  are used. The motivating idea in those methods is that  $P_{\text{noise}}$   
 122 is used to identify and locate targets and that  $P_{\text{signal}}$  is used to deliver quantitative in-  
 123 formation about the target. However, there is a more generally useful reason to include  
 124 both projections. By considering both  $P_{\text{noise}}$  and  $P_{\text{signal}}$ , one can introduce a continu-  
 125 ous weighting in terms of a user-defined parameter  $\epsilon > 0$  according to

$$\begin{aligned} I_\epsilon(\mathbf{y}) &= \left[ \sum_{n=1}^N \epsilon^{-1} \|P_{\text{noise}}\mathbf{a}_n(\mathbf{y})\|^2 + \|P_{\text{signal}}\mathbf{a}_n(\mathbf{y})\|^2 \right]^{-1} \\ &= \epsilon \left[ \sum_{n=1}^N \left( 1 - (1 - \epsilon) \frac{|\tilde{U}^H \mathbf{a}_n(\mathbf{y})|^2}{\|\mathbf{a}_n(\mathbf{y})\|^2} \right) \|\mathbf{a}_n(\mathbf{y})\|^2 \right]^{-1}, \end{aligned} \quad (8)$$

126 where we have resubstituted our expressions for  $P_{\text{noise}}$  and  $P_{\text{signal}}$  into (8).

127 For a single target located at  $\mathbf{y}_0$ , we have found in a neighborhood about  $\mathbf{y}_0$  that

$$\frac{|\tilde{U}^H \mathbf{a}_n(\mathbf{y})|^2}{\|\mathbf{a}_n(\mathbf{y})\|^2} \approx 1 - \beta^2 |\mathbf{y} - \mathbf{y}_0|^2 \quad (9)$$

128 for some  $\beta$  (Kim & Tsogka, 2021). Consider the simple function  $f(x) = 1 - \beta^2 x^2$ . It  
 129 assumes its maximum value of 1 on  $x = 0$ . It assumes its full-width/half-maximum (FWHM)  
 130 on  $\Delta x^* = \pm 1/(\sqrt{2}\beta)$ . Now consider the function,

$$F_\epsilon(x) = \frac{\epsilon}{1 - (1 - \epsilon)f(x)}. \quad (10)$$

131 This function also assumes its maximum value of 1 on  $x = 0$ , but it assumes its FWHM  
 132 on

$$\Delta x^* = \pm \frac{\sqrt{\epsilon}}{\beta\sqrt{1 - \epsilon}} = \frac{\sqrt{\epsilon}}{\beta} + O(\epsilon^{3/2}), \quad \epsilon \rightarrow 0. \quad (11)$$

133 Thus for a function  $f(x)$  with some FWHM, we can instead consider the function  $F_\epsilon(x)$   
 134 given in (10) with the same FWHM, but scaled by  $\sqrt{\epsilon}$ . It is through this simple mech-  
 135 anism that we have determined that this generalization of MUSIC for SAR has a range  
 136 resolution that is  $O(\sqrt{\epsilon}(c/B)(L/R))$  and a cross-range resolution that is  $O(\sqrt{\epsilon}(c/B)(L/a))$ .

137 The key point is the factor of  $\sqrt{\epsilon}$  since  $\epsilon$  can be made arbitrarily small. This tun-  
 138 able resolution can be used advantageously when forming images of targets. For exam-  
 139 ple, the value of  $\epsilon$  can be varied by the user based on the resolution of the mesh used  
 140 to sample the imaging region. Upon identifying subregions where an individual target  
 141 is located, one can then change the value of  $\epsilon$  to obtain a very high resolution image of  
 142 the target on a finer mesh.

#### 143 4 Modified Kirchhoff Migration

144 The traditional method for SAR imaging uses Kirchhoff Migration (KM). This imag-  
 145 ing method is robust to measurement noise. In fact, it is not restricted like MUSIC to  
 146 problems where the signal subspace can be reliably distinguished from the noise subspace.  
 147 For that reason, KM is robust for problems with very low SNR. Here, we give a mod-  
 148 ification of KM based off of what we have done for MUSIC to yield a KM imaging method  
 149 with tunable resolution.

150 Using the data defined in (1), we form the KM image through evaluation of

$$I^{\text{KM}}(\mathbf{y}) = \sum_{n=1}^N \sum_{m=1}^{2M-1} d_n^*(\omega_m) e^{i2\omega_m |\mathbf{x}_n - \mathbf{y}|/c}, \quad (12)$$

151 with  $d_n^*(\omega_m)$  denoting the complex conjugate of  $d_n(\omega_m)$ . It is well known that the res-  
 152 olution of  $I^{\text{KM}}$  is  $O(c/B)$  in range and  $O(\lambda L/a)$  in cross-range.

153 The inner sum over frequencies in (12) is an inner product, so it can be interpreted  
 154 as a projection of the illumination vector

$$\mathbf{a}_n(\mathbf{y}) = \left[ e^{i2\omega_1 |\mathbf{x}_n - \mathbf{y}|}, \dots, e^{i2\omega_{2M-1} |\mathbf{x}_n - \mathbf{y}|} \right]^T, \quad (13)$$

onto the data vector

$$\mathbf{d}_n = [d_n(\omega_1), \dots, d_n(\omega_{2M-1})]^T, \quad (14)$$

or

$$I^{\text{KM}}(\mathbf{y}) = \sum_{n=1}^N \mathbf{d}_n^H \mathbf{a}_n(\mathbf{y}). \quad (15)$$

Let  $\mathbf{d}_n = \hat{\mathbf{d}}_n \|\mathbf{d}_n\|$  and  $\mathbf{a}_n(\mathbf{y}) = \hat{\mathbf{a}}_n(\mathbf{y}) \|\mathbf{a}_n(\mathbf{y})\|$ . Just as we have done for MUSIC, we  
 form a tunable KM imaging functional through evaluation of

$$I_\epsilon^{\text{KM}}(\mathbf{y}) = \epsilon \left| \sum_{n=1}^N \left( 1 - (1 - \epsilon) \hat{\mathbf{d}}_n^H \hat{\mathbf{a}}_n(\mathbf{y}) \right) \right|^{-2}. \quad (16)$$

155 This modification of KM will yield an image with a tunable resolution that scales as  $\sqrt{\epsilon}$ .  
 156 We expect that this imaging method will have a range resolution that is  $O(\sqrt{\epsilon}c/B)$  and  
 157 a cross-range resolution that is  $O(\sqrt{\epsilon}\lambda_0 L/a)$ . Since  $\epsilon$  is a user-defined parameter, it can  
 158 be made arbitrarily small to produce a very high-resolution image.

159 The mechanism through which (16) achieves high resolution requires that  $\hat{\mathbf{d}}_n^H \hat{\mathbf{a}}_n(\mathbf{y}) =$   
 160 1 on target locations. When considering an imaging region with multiple targets, this  
 161 requirement may not be met exactly on all target locations. Therefore, (16) may not clearly  
 162 identify some of the targets. However, if (16) is used in a sub-region containing a sin-  
 163 gle target, it will produce tunable high-resolution images of that individual target.

#### 164 5 Numerical results

165 We use numerical simulations to test and evaluate the imaging method presented  
 166 above. We used the following values for the system parameters which are based on the

167 GOTCHA data set (Casteel Jr et al., 2007). We set the origin of a coordinate system  
 168 in the middle of a 4.8 m  $\times$  4.8 m imaging region situated at ground level,  $z = 0$ . The  
 169  $x$ -coordinate is cross-range and the  $y$ -coordinate is range. The coordinates along the linear  
 170 flight path where measurements are taken are  $\mathbf{x}_n = (x_n, R, H)$  with  $x_n = -a/2 +$   
 171  $a(n - 1)/(N - 1)$  for  $n = 1, \dots, N$ . Here, the range of the flight path is  $R = 7.10$  km  
 172 and the height is  $H = 7.30$  km, so that  $L = \sqrt{H^2 + R^2} = 10.18$  km. The length of  
 173 the synthetic aperture is  $a = 0.13$  km. The central frequency is  $f_0 = 9.6$  GHz and the  
 174 bandwidth is  $B = 622$  MHz. Using  $c = 3 \times 10^8$  m/s, we find that the central wave-  
 175 length is  $\lambda_0 = 3.12$  cm. We use  $M = 31$  equi-spaced frequencies over the bandwidth  
 176 and  $N = 124$  spatial measurements.

### 177 5.1 Single target

178 We first apply the imaging method to a single point target located at  $\mathbf{y}_0 = (1 \text{ m}, 1 \text{ m}, 0)$ .  
 179 We added measurement noise to the measured signal so that  $\text{SNR} = 15.3989$  dB. The  
 180 image resulting from applying KM given in (12) appears in the left plot and the image  
 181 resulting from applying the modified KM given in (16) appears in the right plot of Fig. 2.  
 182 For both plots, the image was normalized by its peak value and plotted in dB ( $10 \log_{10}$ -  
 183 scale). Additionally, the images are centered about the true target location.

184 Using the parameter values for this problem, we find that  $c/B \approx 15 \lambda_0$  and  $\lambda_0 L/a \approx$   
 185  $79 \lambda_0$  corresponding to the range ( $x$ ) and cross-range ( $y$ ) resolutions, respectively. The  
 186 left plot shows a peak at the target location whose full-width/half-maximum (FWHM)  
 187 corresponds to those resolutions estimates. Additionally, we see the familiar side-lobes  
 188 that appear in KM images.

189 To form the image appearing the right plot of Fig. 2, we have used  $\epsilon = 10^{-4}$  in  
 190 the modified KM image. This image has a sharper peak at the target location with no  
 191 apparent side-lobes. It has a much higher resolution than the KM image with less ar-  
 192 tifacts.

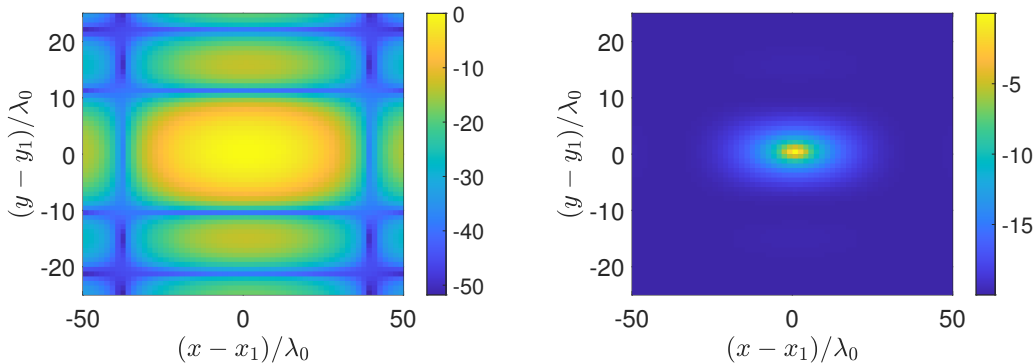


**Figure 2.** (Left) Image formed by KM centered on the target location, normalized by its peak value and plotted in dB ( $10 \log_{10}$ -scale) with  $\text{SNR} = 15.3989$  dB. (Right) Image formed using modified KM with  $\epsilon = 10^{-4}$  for the same measurement data.

193 We expect that the image resolution of modified KM to be  $O(\sqrt{\epsilon c}/B)$  in range and  
 194  $O(\sqrt{\epsilon} \lambda_0 L/a)$  in cross-range. Using numerical simulations, we estimate the FWHM in range  
 195 and cross-range for noiseless data for the same single target. The image resolution re-  
 196 sults are shown in Fig. 3. The plots in Fig. 3 show the computed FWHM in range ( $\Delta x^*/\lambda_0$ )  
 197 as blue circles, and in cross-range ( $\Delta y^*/\lambda_0$ ) as red squares. The left plot in Fig. 3 shows  
 198 the FWHM results as a function of  $\epsilon$  with  $c/B$  and  $\lambda_0 L/a$  fixed. The center plot shows

199 FWHM results as a function of  $c/B$  with  $\epsilon = 10^{-4}$  and  $\lambda_0 L/a$  fixed. The right plot shows  
 200 FWHM results as a function of  $\lambda_0 L/a$  with  $\epsilon = 10^{-4}$  and  $c/B$  fixed. All three of these  
 201 plots show linear fits to the data as solid curves. The black dashed curve shows the ex-  
 202 pected behavior of the image resolution. These results verify the resolution estimates for  
 203 modified KM.

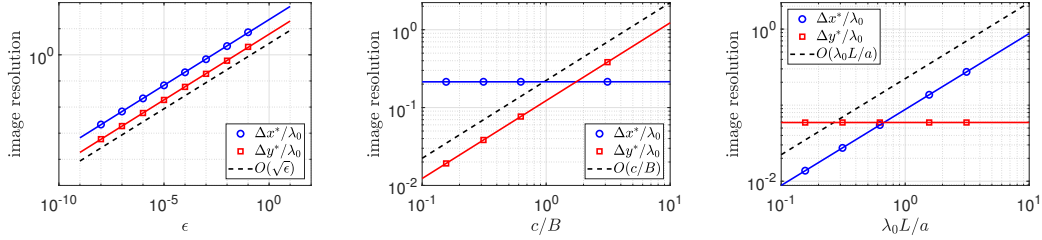


**Figure 3.** Computed full-width/half-maximum (FWHM) values of images produced with modified KM as a function of  $\epsilon$  (left),  $c/B$  (center), and  $\lambda_0 L/a$  (right).

## 204 5.2 Multiple targets

205 We now consider an imaging scene with three identical targets. The targets are lo-  
 206 cated at  $\mathbf{y}_1 = (-1.4 \text{ m}, -0.5 \text{ m}, 0 \text{ m})$ ,  $\mathbf{y}_2 = (-0.6 \text{ m}, -1.2 \text{ m}, 0 \text{ m})$ , and  $\mathbf{y}_3 = (1.2 \text{ m}, 1.1 \text{ m}, 0 \text{ m})$ .  
 207 The image formed using KM is shown in the left plot and the imaged formed using mod-  
 208 ified KM is shown in the right plot of Fig. 4. Measurement noise was added to the sig-  
 209 nals so that  $\text{SNR} = 14.1217 \text{ dB}$ . The KM image shows peaks at the target locations  
 210 indicated as red “+” symbols. However, the interactions of the side-lobes yields several  
 211 imaging artifacts. In contrast, the modified KM image is free from imaging artifacts and  
 212 identifies sharp regions where the targets are located.

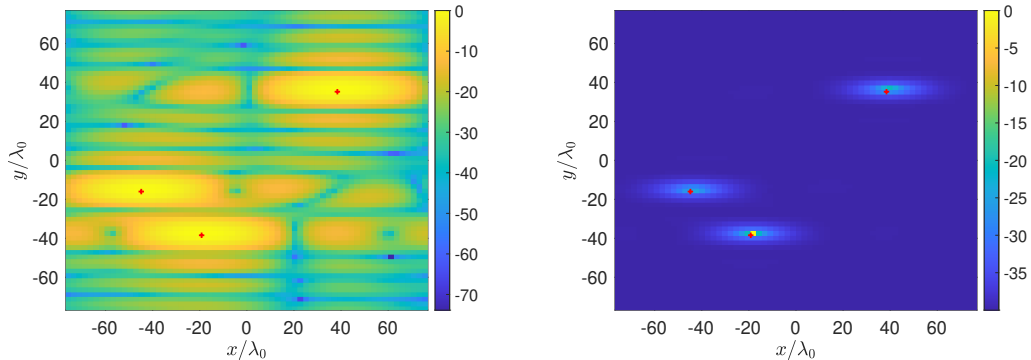


**Figure 4.** (Left) Image formed by KM normalized by its peak value and plotted in dB ( $10 \log_{10}$ -scale) with  $\text{SNR} = 14.1217 \text{ dB}$ . (Right) Image formed using modified KM with  $\epsilon = 10^{-4}$  for the same measurement data.

213 A challenge in using the modified KM is that it relies on an exact cancellation at  
 214 a peak value that is normalized to one. When there are multiple targets and the KM im-  
 215 age is normalized by its maximum value, presumably on only one of those targets incurs  
 216 this exact cancellation. Consequently, the image of the other targets may not be as sharp.  
 217 However, using the image shown on the right plot of Fig. 4, one can identify small sub-

218 regions where each of the three targets are located. If we were to evaluate the modified  
 219 KM in each of these sub-regions, we expect to obtain high-resolution images of the in-  
 220 dividual targets because each of those images would be normalized by the maximum value  
 221 in the small sub-region corresponding to the individual target.

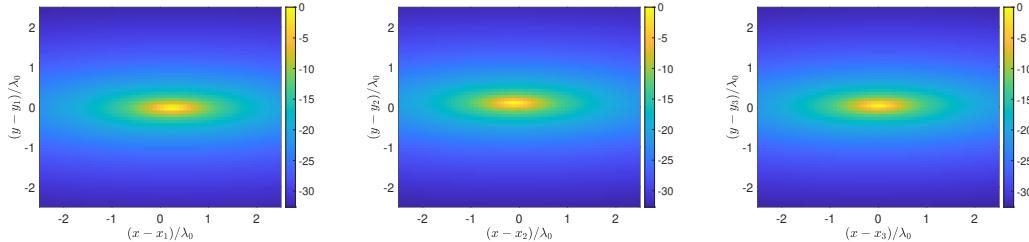


**Figure 5.** Close-up images of target 1 (left), target 2 (center), and target 3 (center) in a small  $5\lambda_0 \times 5\lambda_0$  sub-region about the target location, using the same data used in Fig. 4. Each image is centered about the true target location and normalized by its maximum value.

222 In Fig. 5 we plot close-up images in a  $5\lambda_0 \times 5\lambda_0$  sub-region centered about the true  
 223 location of target 1 (left), target 2 (center), and target 3 (right) using  $\epsilon = 10^{-4}$ . The  
 224 images are formed using the same data used in Fig. 4. The only difference is evaluat-  
 225 ing the modified KM only in a small sub-region. These images demonstrate the very high  
 226 resolution achievable using modified KM. Moreover, the resolution achieved by this method  
 227 is set by the user-defined parameter  $\epsilon$ .

228 The results in Fig. 5 show that the images are not peaked at the exact target loca-  
 229 tions. They are misaligned by fractions of a wavelength. Because modified KM yields  
 230 such high-resolution images of targets compared with KM, we find that it shows how noise  
 231 affects KM, and hence modified KM. The images produced by KM and modified KM when  
 232 we increase the noise such that  $\text{SNR} = 4.1217$  dB are shown in Fig. 6. The relative per-  
 233 formance of both of these imaging methods appears to be the same as for the higher SNR  
 234 case shown in Fig. 4. However, the plots of close-up images about each of the target  
 235 locations shown in Fig. 7 using the high-resolution modified KM images show that the peaks  
 236 are farther away from the true target locations than for the higher SNR case shown in  
 237 Fig. 5, on the order of a wavelength. We see that this effect is more pronounced in cross-  
 238 range than in range.

239 With very low SNR, the noise affects the phase of the measured signals in the form  
 240 of random phase rotations. These phase rotations shift the predicted location of targets  
 241 slightly. When plotting images using KM, the image resolution is too coarse to be able  
 242 to observe these shifts in target locations. However, with modified KM, the resolution  
 243 is so high that one observes these shifts. Our simulation results suggest that this random  
 244 shifts in the target locations are bounded by a wavelength or less.

## 245 6 Conclusions

246 We have identified the fundamental mechanism leading to tunable high-resolution  
 247 images with our generalization of MUSIC. Using that same mechanism we have intro-  
 248 duced a simple modification to KM. This modification is a rational transformation of the  
 249 normalized KM image that includes a user-defined parameter, which we call  $\epsilon$ , that ef-  
 250 fectively tunes the resolution. We have shown that the resolution of the modified KM  
 251 method is  $O(\sqrt{\epsilon c}/B)$  in range and  $O(\sqrt{\epsilon \lambda_0} L/a)$  in cross-range. Because this user-defined  
 252 parameter can be made arbitrarily small, we can achieve sub-wavelength resolution of

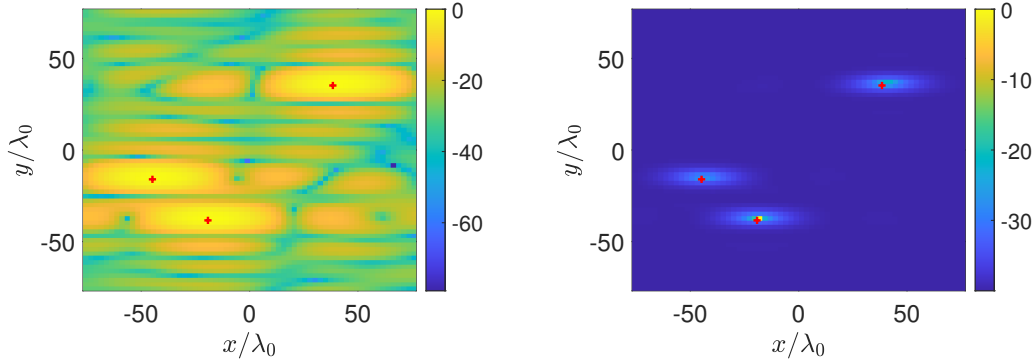


**Figure 6.** (Left) Image formed by KM normalized by its peak value and plotted in dB ( $10 \log_{10}$ -scale) with SNR = 4.1217 dB. (Right) Image formed using modified KM with  $\epsilon = 10^{-4}$  for the same measurement data.

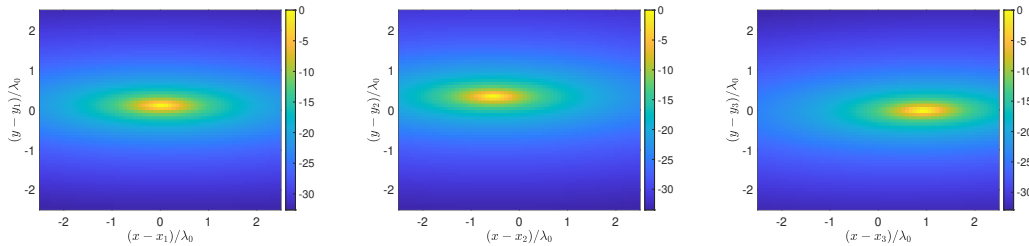


**Figure 7.** Close-up images of target 1 (left), target 2 (center), and target 3 (center) in a small  $5\lambda_0 \times 5\lambda_0$  sub-region about the target location with SNR = 4.1217 dB.

253 targets using this method. In contrast to MUSIC, this modified KM method can be ap-  
 254 plied to measurements with low SNR.

255 When SNR is very low, the modified KM image of targets is shifted from their true  
 256 location. We are able to observe these shifts because the modified KM produces such  
 257 high resolution images. These shifts in the target locations are due to noise causing phase  
 258 perturbations to measurements. In our simulations, we have observed that when SNR  $\approx$   
 259 0 dB, these shifts are on the order of a wavelength.

260 Because this modified KM method can be applied with no additional cost beyond  
 261 the KM method, itself, and because it produces tunable, high-resolution images, we be-  
 262 lieve that this method is very useful for a broad variety of SAR imaging problems.

### 263 Acknowledgments

264 The authors acknowledge support by the Air Force Office of Scientific Research (FA9550-  
 265 21-1-0196). A. D. Kim also acknowledges support by the National Science Foundation  
 266 (DMS-1840265).

### 267 References

268 Casteel Jr, C. H., Gorham, L. A., Minardi, M. J., Scarborough, S. M., Naidu, K. D.,  
 269 & Majumder, U. K. (2007). A challenge problem for 2d/3d imaging of tar-  
 270 gets from a volumetric data set in an urban environment. In *Algorithms for*  
 271 *synthetic aperture radar imagery xiv* (Vol. 6568, p. 65680D).

- 272 Cheney, M. (2001). A mathematical tutorial on synthetic aperture radar. *SIAM Re-*  
273 *view*, 43(2), 301–312.
- 274 Cheney, M., & Borden, B. (2009). *Fundamentals of Radar Imaging* (Vol. 79).  
275 SIAM.
- 276 Doerry, A. W. (2006). *Performance limits for synthetic aperture radar – second edi-*  
277 *tion* (Tech. Rep. No. SAND2006-0821). Sandia National Laboratories.
- 278 González-Rodríguez, P., Kim, A. D., & Tsogka, C. (2021). Quantitative signal sub-  
279 space imaging. *Inverse Probl.* doi: 10.1088/1361-6420/ac349b
- 280 Kim, A. D., & Tsogka, C. (2021). *High-resolution, quantitative signal subspace imag-*  
281 *ing for synthetic aperture radar*.
- 282 Moreira, A., Prats-Iraola, P., Younis, M., Krieger, G., Hajnsek, I., & Papathanas-  
283 siou, K. P. (2013). A tutorial on synthetic aperture radar. *IEEE Geosci.*  
284 *Remote Sens. Mag.*, 1(1), 6–43.
- 285 Prony, G. R. B. (1795). Essai experimental et analytique sur les lois de la dilatalrlite  
286 de fluids elastiques et sur cells de la vapeur de l’alcool, à différents tempoera-  
287 tures. *J. de l’Ecole Polytech.*, 1, 24–76.